A hard x-ray nanoprobe for scanning and projection nanotomography

Pierre Bleuet,[1,2] Peter Cloetens,[1] Patrice Gergaud,[2] Denis Mariolle,[2] Nicolas Chevalier,[2] Rémi Tucoulou,[1] Jean Susini,[1] and Amal Chabli[2]
[1]*European Synchrotron Radiation Facility, BP 220, 38043 Grenoble Cedex, France*
[2]*CEA, LETI, MINATEC, F38054 Grenoble, France*

(Received 28 January 2009; accepted 23 March 2009; published online 7 May 2009)

To fabricate and qualify nanodevices, characterization tools must be developed to provide a large panel of information over spatial scales spanning from the millimeter down to the nanometer. Synchrotron x-ray-based tomography techniques are getting increasing interest since they can provide fully three-dimensional (3D) images of morphology, elemental distribution, and crystallinity of a sample. Here we show that by combining suitable scanning schemes together with high brilliance x-ray nanobeams, such multispectral 3D volumes can be obtained during a single analysis in a very efficient and nondestructive way. We also show that, unlike other techniques, hard x-ray nanotomography allows reconstructing the elemental distribution over a wide range of atomic number and offers truly depth resolution capabilities. The sensitivity, 3D resolution, and complementarity of our approach make hard x-ray nanotomography an essential characterization tool for a large panel of scientific domains. © *2009 American Institute of Physics.*
[DOI: 10.1063/1.3117489]

I. INTRODUCTION

Micro- and nanofabrication steps typically involve optical lithography, thin film physical or chemical deposition, or etching processes from which systems as small as a few nanometers can be built. These systems include (micrometer and nanometer sized) wires, electromechanical systems (MEMS and NEMS), integrated circuits, photonics, or sensors that are extremely quickly increasing in complexity. To analyze and refine the successive fabrications steps and validate the microsystem conception and efficiency, it is necessary to use and control complementary characterization tools. The most widely used are briefly listed hereafter. Electronic and atomic interactions are used in transmission and scanning electron microscopy[1,2] (TEM and SEM), electron energy loss spectroscopy,[3] atomic and kelvin force microscopy[4] (AFM), and provide two-dimensional (2D) images with (sub) nanometer spatial resolution. Ion beams are used in focused ion beam,[5] secondary ion mass spectroscopy,[6] or medium energy ion scattering[7] to analyze trace elements in a fully destructive way. None of these techniques can achieve nondestructive and depth-resolution information.

A large number of techniques are based on x-rays; among them one can cite x-ray photoelectron spectroscopy[8,9] (high energy or angle resolved), x-ray diffraction and fluorescence (XRD and XRF), and x-ray computed tomography.[10,11] X-rays are good candidates for sample characterization because (i) they are to a large extent nondestructive, (ii) they give quantitative access to a number of physical properties of a specimen, (iii) they can penetrate hundreds of micrometers thick samples, and (iv) they do not require specific sample preparation with respect to the aforementioned electron or atomic microscopes. However, they were suffering until the last few years from a relatively coarse spatial resolution that prevented their use for micro- and nanotechnology imaging—a scientific field extremely spatial resolution demanding. Great improvements in x-ray optics lead to the fabrication of focusing devices and lenses allowing few tens of nanometer resolution in the soft x-ray regime (up to few keV) for three-dimensional (3D) characterization.[12–15] For hard x-rays, i.e., energies higher than 10 keV, reaching that resolution is more challenging because of the complexity in manufacturing high efficiency and stable x-ray focusing optics. Several schemes have been proposed to focus hard x-rays, based on refractive, reflective, or diffractive optics. Among them, Kirkpatrick–Baez (KB) mirrors[16] offer the best compromise since they are the most efficient (typically higher than 50%) and they are achromatic while keeping reasonable working distances of the order of a few centimeters. A KB-based hard x-ray nanoprobe coupled with a third generation synchrotron source has been developed at the European Synchrotron Radiation Facility in Grenoble, France and is described elsewhere.[17,18] In this work we explore the possibilities offered by such a nanoprobe in terms of multimodal fully 3D tomography at decananometer resolution for micro- and nanotechnologies characterization. Although previous reports exist that present nanotomography results with hard x-rays,[19–21] no studies show 3D chemical and morphological images at such a spatial resolution.

II. EXPERIMENTAL SETUP

Figure 1 shows a schematic view of the experimental setup. The x-ray beam is focused at an energy of 17.5 keV by multilayer coated KB optics to a beam with lateral dimensions of 80 nm by 120 nm. The sample is mounted as it is on top of a five-axis sample stage. For tomography analysis, the experimental procedure can be divided in four successive steps. First, the sample is aligned with respect to the axis of rotation in projection mode. To do so the sample is moved

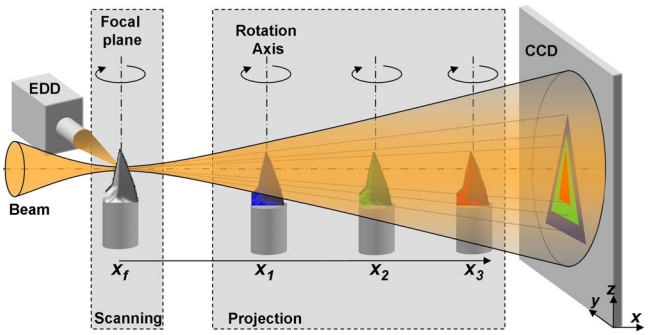

FIG. 1. (Color online) Scanning and projection nanotomography acquisition schemes.

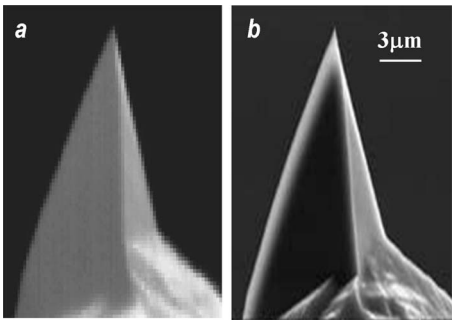

FIG. 2. (a) Distribution of Pt of a coated AFM tip measured with the x-ray scanning nanoprobe. (b) SEM micrograph provided by Nanosensor Co. (with their agreement).

out of the focal plane and magnified radiographs are recorded at 0°, 90°, and 180° at a maximum field of view of 700 μm. Then the sample is brought as close as possible to the axis of rotation and the alignment is iteratively refined at higher magnification (i.e., smaller focus to sample distance). Once the sample is aligned, a complete holotomography scan is performed.[11,18] It consists in a series of four tomography scans at different focus-sample distances in projection mode to fulfill the phase retrieval conditions.[11] The 100 nm KB spot size is actually used as an x-ray source while x-ray projections are recorded by a fast readout and low noise in-house system.[22] The pixel resolution of the detector system is 2.4 μm and it is set at a fixed distance of 1.22 m downstream of the focus. The focus-sample distances used are 30.5, 31.5, 35.5 and 45.5 mm, resulting in a final voxel resolution of 60 nm and a field of view of 90 μm. For each distance 1499 projections over a complete turn are recorded. The full holotomography scan takes about 5 h to be completed. To switch to the scanning mode and access to chemical analysis, the sample is brought back into the focus. No sample realignment is necessary. Fluorescence nanotomography is then performed as described in the literature at the micrometer scale.[23–25] The sample is raster scanned in the focal plane and the fluorescence is recorded pixel by pixel with an energy dispersive detector. The scanning time is much higher than in projection mode: a complete single-slice acquisition takes about 30 min with a 100 ms exposure time, 175 points per line each 200 nm (i.e., a 35 μm scan) and 90 angles over a full turn. To get 3D images, this operation has to be repeated at different heights, potentially leading to scanning times within the day range. All along the continuous scan of the sample, fluorescence spectra are recorded and then processed for 3D reconstruction. 3D fluorescence reconstructions were obtained by stacking 2D reconstructions from circular scans.

III. RESULTS

To demonstrate the 3D possibilities offered by ID22NI, an AFM commercial tip (Nanosensor, PointProbe® series) has been analyzed. The silicon tip is itself mounted on a cantilever made also of silicon. The whole assembly is coated with a thin adhesion layer of chromium and with a 25 nm thick platinum/iridium layer. 2D XRF multispectral maps have been recorded and fitted to provide elemental distributions. Figure 2 shows both XRF (the 2D platinum distribution) and SEM (provided by Nanosensor) images of the tip. Obviously, the SEM image quality is by far better than the XRF one, thanks to a resolution one order of magnitude higher; however, the figure shows that both characterization tools give compatible and complementary information.

Figure 3 shows reconstructions (slices and full object) for both scanning fluorescence tomography and projection holotomography. The slices show a platinum layer covering a silicon bulk tip. The chemical discrimination is ensured by fluorescence tomography. In holotomography, the density distribution is reconstructed. Using a 3D region growing segmentation algorithm, two distinct regions with different densities (but no specific chemical signatures) can be segmented. 3D reconstructions have also been computed for both techniques; similar remarks can be done. In both cases, the capping platinum layer appears to be a few pixels thick, although it is supposed to be only 25 nm. In fluorescence tomography, the reason is twofold. First this is a scanning method, much more demanding in terms of mechanical long-term stability and repeatability. The current instrumentation may degrade the resolution and provoke a thickening of the layer. Second, this method does not profit from geometrical magnification as in holotomography. The resolution is beam size limited; the latter is measured using standard knife-edge techniques on a test pattern and appears to be 100 nm.[26] In holotomography, image quality looks better because scanning time and instrumentation issues are slightly less demanding, and the magnification geometry allows sampling the volume down to 60 nm. Still, the layer appears to be about 3 pixels wide, which correspond to about 180 nm instead of the expected 25 nm. Here again, the reason must be

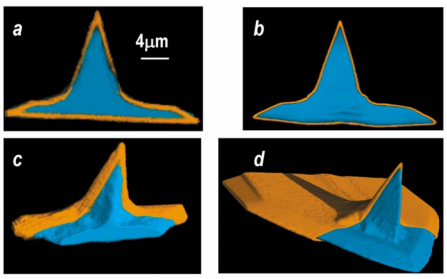

FIG. 3. (Color online) (a) Fluorescence tomography reconstructed slice with chemical identification. Platinum is in orange (external layer) and silicon in blue. (b) Holotomography color-coded image of the same slice; the image has been segmented into two regions having different densities. (c) 3D chemical image. (d) 3D density image.

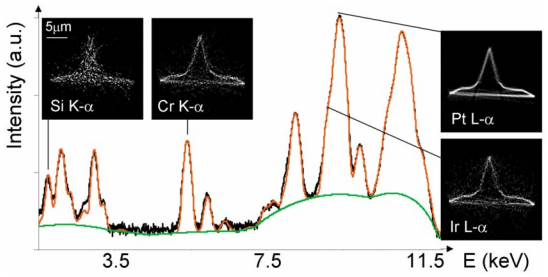

FIG. 4. (Color online) Total fluorescence spectrum and 2D elemental images of one reconstructed slice. Experimental data (black, noisy), fitted background (green), and fitted fluorescence peaks (red, noiseless). Nonindexed peaks are *M* lines, *K*-β, and *L*-β lines.

found in potential miscalibrations, e.g., vibration or sample wobbling, that end-up with a degradation of the global point-spread-function of the system. For both methods, it is foreseen to develop in-line metrology[27] to be able to quantify the geometrical calibration and either improving it using specific positioning devices or proceeding to a precalibration of images using fiducial markers as it is done in TEM tomography.[28]

Fluorescence tomography allows a thorough investigation of the different chemical phases. Figure 4 shows the global fluorescence spectrum obtained by summing all the fluorescence spectra measured all along the scan; it allows fast identification of the chemical elements and can be fitted using for example the PYMCA software package.[29] Some elemental reconstructions are also displayed. It should be noticed that although highly absorbed by the platinum layer, the air, and the detector beryllium window, the underneath pure silicon object can still be reconstructed. Chromium (25 nm thick) and iridium (after fitting for discrimination from Pt) can also be reconstructed; platinum is giving the highest contrast.

IV. CONCLUDING REMARKS

It is worth noting that both analyses can be performed on the same instrument, i.e., within the same geometrical coordinate frame. To further speed up the acquisition process, a spiral scan[25] can be used.

Although the lateral resolution of hard x-ray microscopes is still limited with respect to electron microscopes, great efforts are being done to make both techniques.Besides the ultimate spot size achievement, the reason of the complexity in achieving hard x-ray nanotomography is twofold. First, measurement times may be long, thus requiring a high level of beam and mechanics stability. Second, to produce artifact-free 3D images, the absolute calibration (positions and angles) of the experimental setup must be precise at the nanoscale and requires development of customized hardware and software.[27] Ongoing developments also include the possibility to perform local tomography, i.e., scanning and reconstructing only a region of interest out of a large sample.

Further extensions of this work include generalization of tomography to other x-ray interactions. In particular, the recently developed scanning XRD tomography method[30] can be transposed to nanoprobes provided the grain size is compatible with the nanometric resolution and the diffracted intensity is sufficiently high. Since the latter is proportional to the atomic number, nanodiffraction tomography may be successfully applied in microelectronics, e.g., for analyzing samples with high *Z* coatings such as platinum, hafnium, or gold. These nondestructive multimodal 3D nanocharacterization tools are essential for further progress in nanotechnology fabrication methods.

[1] L. J. Allen, Nat. Nanotechnol. **3**, 255 (2008).
[2] A. E. Porter, M. Gass, K. Muller, J. N. Skepper, P. A. Midgley, and M. Welland, Nat. Nanotechnol. **2**, 713 (2007).
[3] G. Gensterblum, J. J. Pireaux, P. A. Thiry, R. Caudano, J. P. Vigneron, P. Lambin, A. A. Lucas, and W. Krätschmer, Phys. Rev. Lett. **67**, 2171 (1991).
[4] G. Binnig, C. F. Quate, and C. Gerber, Phys. Rev. Lett. **56**, 930 (1986).
[5] D. Cooper, R. Truche, and J.-L. Rouvière, Ultramicroscopy **108**, 488 (2008).
[6] F. Fillot, S. Maîtrejean, I. Matko, and B. Chenevier, Appl. Phys. Lett. **92**, 023503 (2008).
[7] S. Founta, J. Coraux, D. Jalabert, C. Bougerol, F. Rol, H. Mariette, H. Renevier, B. Daudin, R. A. Oliver, C. J. Humphreys, T. C. Q. Noakes, and P. Bailey, J. Appl. Phys. **101**, 063541 (2007).
[8] A. Bailly, O. Renault, N. Barrett, L. F. Zagonel, P. Gentile, N. Pauc, F. Dhalluin, T. Baron, A. Chabli, J. C. Cezar, and N. B. Brookes, Nano Lett. **8**, 3709 (2008).
[9] O. Renault, N. T. Barrett, D. Samour, and S. Quiais-Marthon, Surf. Sci. **566**, 526 (2004).
[10] F. Adams, Spectrochim. Acta, Part B **63**, 738 (2008).
[11] P. Cloetens, R. Mache, M. Schlenker, and S. Lerbs-Mache, Proc. Natl. Acad. Sci. U.S.A. **103**, 14626 (2006).
[12] D. Attwood, Nature (London) **442**, 642 (2006).
[13] G. Schneider, E. Anderson, S. Vogt, C. Knochel, D. Weiss, M. LeGros, and C. Larabell Surf. Rev. Lett. **9**, 177 (2002).
[14] M. A. Le Gros, G. McDermott, and C. A. Larabell, Curr. Opin. Struct. Biol. **15**, 593 (2005).
[15] P. J. Withers, Mater. Today **10**, 26 (2007).
[16] P. Kirkpatrick and A. V. Baez, J. Opt. Soc. Am. **38**, 766 (1948).
[17] P. Bleuet, A. Simionovici, L. Lemelle, T. Ferroir, P. Cloetens, R. Tucoulou, and J. Susini Appl. Phys. Lett. **92**, 213111 (2008).
[18] R. Mokso, P. Cloetens, E. Maire, W. Ludwig, and J. Y. Buffière, Appl. Phys. Lett. **90**, 144104 (2007).
[19] C. G. Schroer, J. Meyer, M. Kuhlmann, B. Benner, T. F. Günzler, B. Lengeler, C. Rau, T. Weitkamp, A. Snigirev, and I. Snigireva, Appl. Phys. Lett. **81**, 1527 (2002).
[20] H. Toda, K. Uesugi, A. Takeuchi, K. Minami, M. Kobayashi, and T. Kobayashi, Appl. Phys. Lett. **89**, 143112 (2006).
[21] J. Chen, C. Wu, J. Tian, W. Li, S. Yu, and Y. Tian, Appl. Phys. Lett. **92**, 233 (2008).
[22] J.-C. Labiche, O. Mathon, S. Pascarelli, M. A. Newton, G. G. Ferre, C. Curfs, G. Vaughan, A. Homs, and D. Fernandez Carreiras, Rev. Sci. Instrum. **78**, 091301 (2007).
[23] B. Golosio, A. Simionovici, A. Somogyi, L. Lemelle, M. Chukalina, and A. Brunetti, J. Appl. Phys. **94**, 145 (2003).
[24] S. A. Kim, T. Punshon, A. Lanzirotti, L. Li, J. M. Alonso, and J. R. Ecker, Science **314**, 1295 (2006).
[25] B. Golosio, A. Somogyi, A. Simionovici, P. Bleuet, and J. Susini, Appl. Phys. Lett. **84**, 2199 (2003).
[26] R. Ortega, P. Cloetens, G. Devès, A. Carmona, and S. Bohic, PLoS One **2**, e925 (2007).
[27] European Synchrotron Radiation Facility, Science and Technology Programme 2008–2017, available at http://www.esrf.eu/AboutUs/Upgrade/purple-book.
[28] P. A. Midgley, E. P. W. Ward, A. B. Hungría, and J. M. Thomas, Chem. Soc. Rev. **36**, 1477 (2007).
[29] V. A. Sole, E. Papillon, M. Cotte, P. Walter and J. Susini, Spectrochim. Acta, Part B **62**, 63 (2007).
[30] P. Bleuet, E. Welcomme, E. Dooryhée, J. Susini, J.-L. Hodeau, and P. Walter, Nature Mater. **7**, 468 (2008).